

# Preventing Wetting Between Liquid Copper and Solid Steel: A Simple Extraction Technique



KATRIN E. DAEHN, ANDRÉ CABRERA SERRENHO, and JULIAN ALLWOOD

Copper contamination of end-of-life steel scrap is the main barrier to high-quality recycling. Preferential melting of copper from solid steel scrap is a potential extraction technique, which could be integrated into conventional scrap re-melting with little additional energy. However, previous investigations show removal of liquid copper is limited by its adherence to solid scrap. Preventing wetting between liquid copper and steel is essential to enable separation. The carbon content of steel, initial surface oxidation, and applied coatings effect wetting behavior, but have not been systematically studied. In this study, the individual and combined effects of these parameters on wetting behavior in an inert gaseous environment are observed with a heating microscope. Carbon content appears to be the most significant factor: blistering of the oxide scale on medium-carbon steels causes liquid copper to flow rapidly between the oxide and steel substrate. Liquid copper exhibited a stable droplet on low-carbon steel, regardless of the initial level of oxidation. The tested coatings did not consistently improve nonwetting behavior, but impaired the connection between the scale and steel substrate. This study confirms the potential of the preferential melting technique, but further investigation is needed to determine the most robust process conditions to handle diverse, fragmented scrap at an industrial scale.

<https://doi.org/10.1007/s11663-019-01578-0>  
© The Author(s) 2019

## I. INTRODUCTION

COPPER contamination of end-of-life steel scrap has been identified as the main barrier to high-quality steel recycling.<sup>[1]</sup> Copper and steel are combined for applications in vehicles, appliances, and equipment. Conventional scrap preparation uses hammer shredding to fragment and compact these end-of-life products. Subsequent magnetic separation is not completely effective: copper wiring entwined with steel pieces and steel-encased electric motors remain, so significant quantities of copper follow into the steel melt.<sup>[2]</sup> To date, a commercial extraction technique has not been developed, yet residual copper causes metallurgical problems—most notably surface hot shortness.<sup>[3]</sup> High-quality flat steel products have strict copper tolerances, so end-of-life steel scraps are typically recycled to make tolerant, lower-quality long products.<sup>[4]</sup> In the coming decades, new measures for copper control will be necessary to ensure that all end-of-life scraps are recycled into demanded products.<sup>[5]</sup>

An extraction process could be developed to separate copper from steel. The possible separation routes were evaluated by their potential to remove copper, and their specific energy and material input requirements by Daehn *et al.*<sup>[6]</sup> This analysis shows that techniques such as sulfide slagging<sup>[7]</sup> and vacuum distillation<sup>[8]</sup> have received considerable experimental investigation, but are difficult to implement in practice. However, premelt techniques, such as improved physical scrap preparation, appear to be particularly viable. Trommel<sup>[9]</sup> or ballistic sorting systems<sup>[10]</sup> separate steel pieces by size or density to yield scrap with as low as 0.15 wt pct Cu. However, 20 to 30 pct of the steel scrap stream is diverted as copper-rich. To treat heavily contaminated steel scrap and recover pure copper, preferential melting could be relatively simple. Removing external copper before it is dilute within the steel melt requires less energy. The difference in melting points between copper (1083 °C) and steel (1370 °C to 1536 °C)<sup>[11]</sup> is significant, and could be exploited to collect pure, liquid copper from solid steel. Melting is kinetically fast, and assuming the process is integrated into commercially available scrap heating systems (described by Manning and Fruehan<sup>[12]</sup>), this step would require little additional energy. Such a process would prevent additional copper from entering the steel cycle.

Preferential melting to remove copper has not been developed because there are two main practical limitations: the irregular shape of end-of-life scrap, and the adherence of liquid copper to the surface of solid steel.

---

KATRIN E. DAEHN, ANDRÉ CABRERA SERRENHO, and JULIAN ALLWOOD are with the Department of Engineering, University of Cambridge, Trumpington Street, Cambridge CB2 1PZ, UK. Contact e-mail: jma42@cam.ac.uk

Manuscript submitted December 4, 2018.

Article published online May 20, 2019.

Liquid copper could flow into the crevices of fragmented pieces, undermining separation, as described by Katayama *et al.*<sup>[13]</sup> However, process design could overcome this limitation by applying mechanical force, such as shaking and agitation. Adherence behavior determines the force that must be applied to achieve separation, and thus overall feasibility. Therefore, adherence of liquid copper to the solid steel surface must be investigated first.

Previous wettability investigations are relevant to understand the adherence of liquid copper on steel. The wetting behavior of the copper-iron system is well understood, and has been studied extensively for sintering applications.<sup>[14]</sup> Liquid copper will spread over the iron substrate, penetrating grain boundaries, driven by the reduction in surface energy, and diffusing into grains until the maximum solubility of copper in austenitic iron is reached. This mechanism is characterized by Fredriksson *et al.*<sup>[15]</sup> Spreading is observed for most metal/metal combinations, but nonwetting is observed for most metal/oxide combinations. Oxides have a low surface energy and form weak interactions with liquid metal.<sup>[16]</sup> An oxide, or other nonmetallic layer on the steel could be utilized to minimize the adherence of liquid copper, but there is nuance to this idea.

The first study to investigate preferential melting as a means to separate copper from steel was by Brown and Block,<sup>[17]</sup> who statically held samples of copper winding on steel in oxidizing, inert, and reducing atmospheres. They observed entrapment of the liquid copper between the oxide scale and substrate in an oxidizing atmosphere, but observed direct brazing of copper to steel in a reducing atmosphere.

An oxide scale does not permanently prevent wetting, so subsequent studies investigate the influence of the character of the oxide scale. At high temperature, steel forms a complex surface scale of three oxides. Above 570 °C, FeO, wüstite, grows rapidly and has a porous structure, while more compact Fe<sub>3</sub>O<sub>4</sub>, magnetite, and Fe<sub>2</sub>O<sub>3</sub>, hematite, are present in much smaller proportions (~ 4 and 1 pct, respectively at 1000 °C<sup>[18]</sup>) at the outer surface of the scale. Hara *et al.*<sup>[19]</sup> varied CO/CO<sub>2</sub>(g) partial pressures to yield different scales with dominant FeO, Fe<sub>3</sub>O<sub>4</sub>, or Fe<sub>2</sub>O<sub>3</sub> and studied the interaction of liquid copper. The work of adhesion of copper was greatest when FeO was dominant. The authors hypothesized that copper wetted due to the porous structure, but copper could be melted away from steel when compact Fe<sub>2</sub>O<sub>3</sub> and Fe<sub>3</sub>O<sub>4</sub> were present.

Further studies investigate the evolution of wetting behavior as the oxide scale is reduced, dissolved or physically disrupted. Bernardo *et al.*<sup>[20]</sup> varied the compositions of copper alloys and Fe-based substrates in inert and reducing atmospheres with the goal to improve wetting for sintering applications. Nonwetting was observed with copper on a pure Fe substrate in an argon atmosphere, but when any reductants were present in the system, including carbon in 0.5 wt pct C steel, the oxide layer was reduced to allow complete wetting within 60 seconds. Takahira *et al.*<sup>[21]</sup> observed “unusual” wetting behavior of liquid copper on a preoxidized iron sample in a reducing atmosphere. The

liquid metal rapidly proliferated through the porous structure. Liquid copper can also dissolve iron oxide. Eustanthopolus *et al.*<sup>[22]</sup> show the dissolution of Fe<sub>3</sub>O<sub>4</sub> in liquid copper is moderately favorable, to form Fe-O clusters in solution with liquid copper. These clusters develop coulombic interactions with Fe<sub>3</sub>O<sub>4</sub> to promote adsorption at the interface. In the absence of chemical reactions, studies of similar systems show the iron oxide scale is susceptible to the physical penetration of liquid metal. Protsenko and Eustathopoulos<sup>[23]</sup> observed droplets of lead and lead-bismuth alloys (which do not form intermetallics or exhibit solubility with iron), on thin oxide layers present on Fe and steel substrates in a low oxygen partial pressure (pO<sub>2</sub>) environment. Liquid metal penetrated defects in the oxide film (pores, microcracks) and established direct contact with the solid. Shen<sup>[24]</sup> observed liquid tin wetting on iron and found that the iron oxide film was tenacious, even at low pO<sub>2</sub>, but disruption of the oxide allowed for wetting and interfacial reactions.

As can be seen above, the oxide layer is not universally protective. Wetting behavior is highly sensitive to the system conditions (temperature, atmosphere, surface roughness, composition, as reviewed by Komolafe *et al.*<sup>[25]</sup>), but substances can be applied to the substrate surface to control its behavior and reduce sensitivity. Fluxes are commonly applied, and act to dissolve any oxides present to promote wetting. Alternatively, to promote nonwetting, coatings may provide a barrier. Leak and Fine<sup>[26]</sup> applied a range of coatings, organic and inorganic predips, and braze inhibitors, to promote sweating of liquid copper from steel. The most successful were sodium metasilicate (Na<sub>2</sub>SiO<sub>3</sub>), which is chemically inert, and sodium sulfate (Na<sub>2</sub>SO<sub>4</sub>), which modifies the oxidation reaction of steel. The authors submerged motor armatures in a neutral molten salt medium (CaCl<sub>2</sub> and BaCl<sub>2</sub>) and found nearly complete separation of copper from steel when the specified coatings were applied. However, multiple variables could have contributed to this result: the composition of the steel was not stated, the proportion of copper present was high (which promotes liquation), and the motors were shaken to further remove copper. The role these coatings play in achieving nonwetting is not known.

Although existing literature has examined the influence of some factors on the preferential melting of copper from solid steel, the individual and combined effects of steel carbon content, initial surface oxidation, and coatings on effective wetting behavior have not yet been systematically assessed. In this paper, we examine the influence of these parameters on the wetting behavior of liquid copper to begin defining an appropriate process window for preferential melting.

## II. METHODS

To investigate the wetting behavior of copper in different conditions, copper was melted on various steel substrates and the copper droplet was observed with a heating microscope. Subsequent microscopy of the

sample cross sections revealed the character of the nonmetallic surface layer, the interaction of copper with the surface layer and the distribution of copper across the substrate. Experimental procedures—the composition and surface preparations of the various steel substrates (Section II–A), the operating conditions of the heating microscope (Section II–B) and the preparation of the samples for microscopy (Section II–C) are detailed below.

### A. Test Matrix

Figure 1 illustrates the main variables of the wetting system, which determine the interaction at the liquid/solid interface:

- **Environment:** the environment could be gaseous or liquid. Here, the wetting system is observed in a gaseous environment. To maintain an oxide layer, but limit the growth of porous FeO, an inert atmosphere (argon) was chosen as a constant. Residual oxygen was present in the furnace, which reacted with the surface of the steel substrate.
- **Steel composition:** the composition of the steel varies widely in scrap, and this variability will influence iron oxidation and wetting behavior. Carbon content is the most important element because it can reduce the protective oxide layer. Unalloyed low- and medium-carbon steels, representative of the range of carbon contents encountered in practice, were chosen to understand this effect.
- **Surface condition:** The surface condition of the steel scrap also varies in practice, and depends on steel composition, surface treatments, processing history and service conditions. Steel scrap may have a no initial oxide layer (such as galvanized or coated steel, where the surface layer combusts around 800 °C during preheating), or may exhibit a thick initial oxide layer of primarily magnetite from rusting during service. This range was investigated by preparing initially oxidized and initially ground sample surfaces. The surface condition may be further modified by applying a coating. Sodium metasilicate and sodium sulfate are widely available, cheap and nontoxic, so these coatings were applied to the various substrates to understand if they promote nonwetting behavior.

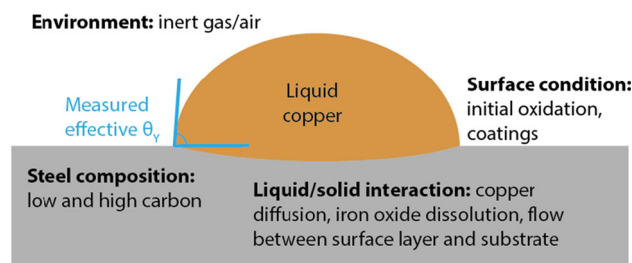


Fig. 1—The copper/steel wetting system showing the variables at the focus of this study.

The test matrix is defined in Table I. Each combination of steel composition, initial surface oxidation, and coating was tested, for a total of 12 distinct tests. Two additional tests were performed as well. To confirm the observations of other researchers, and understand the interaction of copper with the typically observed three-phase oxide layer, one test was performed with low-carbon steel in air. To understand the wetting behavior of copper on a typical surface with no preparation, one test was performed on low-carbon steel in the as-received condition.

Commercially available steels were used for the substrates. For a representative low-carbon, unalloyed steel, CR4-grade was chosen. The CR4 steel was received in the black, cold-rolled condition as a one-mm-thick sheet, which was cut into 10 × 10 mm square pieces. Key steel was chosen to represent an unalloyed medium-carbon steel used in general engineering applications, with a nominal carbon content of 0.35 to 0.45 wt pct. Steel with yet higher carbon content may be encountered in practice, but this medium-carbon steel represents the high-end of carbon content in widespread use. 10 × 10 mm<sup>2</sup> bar from RS Components UK was acquired, from which 1.5-mm-thick sample pieces were cut (all pieces were then ground to a 2500 grit finish—therefore no samples for medium-carbon steel were tested in the “as-received” condition). Optical emission spectroscopy was performed on the CR4 and Key steel to determine their chemical compositions beyond the nominal specifications. The compositions as determined by the average of three sparks are shown in Table II.

To simulate steel scrap with a thick oxide layer formed in service at room temperature, the samples were treated in a box furnace in air at 500 °C for 24 hours to form a scale of Fe<sub>3</sub>O<sub>4</sub>.<sup>[18]</sup> To simulate steel with a minimal initial oxide layer, the samples were ground with sandpaper to 2500 grit and ultrasonically cleaned in water and rinsed with ethanol immediately before testing. Iron oxide forms on the surface of iron at room temperature rapidly after exposure to the atmosphere.<sup>[27]</sup> Therefore, a thin initial oxide layer was present on these ground samples.

To apply the coatings, sodium sulfate (Na<sub>2</sub>SO<sub>4</sub> anhydrous, from Fisher Scientific UK) and sodium metasilicate (Na<sub>2</sub>SiO<sub>3</sub>, from Sigma Aldrich UK) solutions were prepared, as described in the patent by Leak and Fine.<sup>[28]</sup> 15 g of Na<sub>2</sub>SO<sub>4</sub>/Na<sub>2</sub>SiO<sub>3</sub> was mixed with 65 mL of water, and the solution was stirred on a hot plate for about 10 minutes at 60 °C to achieve dissolution. The steel samples were submerged into the solution and dried for about a minute under a hair dryer. The Na<sub>2</sub>SO<sub>4</sub> coating left a white residue, while Na<sub>2</sub>SiO<sub>3</sub> was present on the surface as a glassy gel.

Commercially available copper wiring from wires.co.uk (99.95 pct purity) was used for the copper droplet. 2.64 mm diameter bare copper wire was cut to 2.5 mm length pieces, each weighing 120 to 140 mg. All pieces were ultrasonically cleaned in water and rinsed with ethanol prior to testing to remove surface contaminants; however, a thin layer of copper oxide remained on the surface. Oxygen, either in solution with copper or in the

form of copper oxide, affects the surface tension and wetting behavior of liquid copper, as characterized by Gallois and Lupis.<sup>[29]</sup> Copper wiring with a native surface oxide layer would be encountered in practice, so the condition studied here is relevant.

### B. Droplet Observation

The aptitude of a liquid to wet a solid surface can be characterized by the shape of the liquid droplet. The sessile drop technique is a standard experimental method to measure droplet shape—most commonly Young’s contact angle,  $\theta_Y$ , formed at the contact of the liquid, vapor and solid phases,<sup>[30]</sup> as shown in Figure 1. The condition for wetting is defined as  $\theta_Y < 90$  deg.

To observe the droplet, a Misura HSM2 heating microscope was used. The schematic is shown in Figure 2. The steel substrates were placed on the ends of two alumina sheaths, suspended within the furnace cavity. A thermocouple measured the temperature at the end of one of the alumina sheaths. The light source (a 50 W halogen spotlight bulb) illuminated the sample on one end, while a camera imaged the droplet profile through a transparent quartz screen. Argon (from Air Products BIP, N6.0 purity) flowing at a rate of

0.2 L/min was purged through the furnace cavity (200 × 18 mm diameter) and furnace inlet tube (40 × 3 mm diameter) for 60 minutes prior to testing with the sample in the chamber, and flowed at the same rate during testing. A transparent quartz screen was secured at the end of the inlet tube, with a gap of 3 mm between the screen and the tube. As the furnace cavity was not sealed, some oxygen was present in the system, which we estimate to be in the range of  $10^{-4}$  to  $10^{-3}$  atm.<sup>[31]</sup> The oxygen partial pressure to prevent the oxidation of iron at 1000 °C is extremely low, at  $10^{-12}$  atm.<sup>[32]</sup> A piece of metallurgical coke (approximately 12 × 12 × 3 mm) was placed in the inlet tube, about 10 mm in front of the sample holder. Under flowing argon, the piece of coke had limited contact with oxygen for any substantial reaction, but CO(g) and CO<sub>2</sub>(g) may have formed,<sup>[33]</sup> the ratio of which would have had a reducing or oxidizing effect.<sup>[34]</sup> These conditions were intended to approximate an inert industrial furnace. The atmosphere during testing remained oxidizing, evidenced by the surface oxide formed on all samples and decarburization of the medium-carbon steel. Instrumentation or CO/CO<sub>2</sub> gas mixtures can be used to directly measure and control oxygen concentration. The present apparatus was not equipped with these capabilities, so this is recommended for future analysis. The in-air test

**Table I. The Varied Characteristics Between the Different Steel Substrates**

Steel Composition	Surface Condition					
	Initial Oxidation			Coating		
Low carbon	medium carbon	ground	oxidized	none	Na <sub>2</sub> SO <sub>4</sub>	Na <sub>2</sub> SiO <sub>3</sub>

Each combination was tested in an inert atmosphere, for a total of 12 distinct tests.

**Table II. Chemical Compositions of the Low- and Medium-Carbon Steel Substrates**

Steel Type	Element (Wt Pct)									
	C	N	Si	Mn	P	S	Cr	Ni	Mo	Al
Low carbon	0.08	0.006	0.014	0.14	0.012	0.011	0.031	0.035	0.0058	0.039
Medium carbon	0.39	0.012	0.24	0.74	0.017	0.023	0.189	0.170	0.044	0.0012

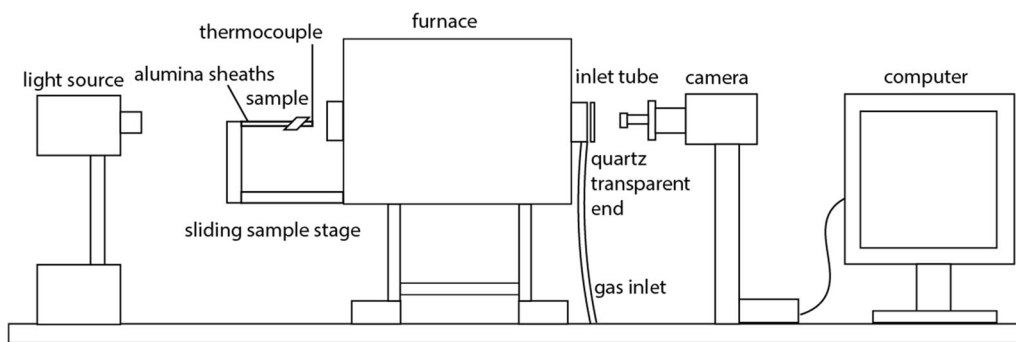


Fig. 2—Schematic of the Misura HSM2 heating microscope.

was run by flowing compressed air through the furnace, also at 0.2 l/min (the piece of metallurgical coke was removed for this test).

The same heating profile was applied during each test. The sample was heated from 20 to 1000 °C at a rate of 50 °C/min, and from 1000 to 1150 °C at 5 °C/min. One snapshot was taken at each degree, from 1000 to 1150 °C. The contact angles of both sides of the droplet were later measured manually using ImageJ software. In some cases, the copper wetting was rapid—the thermal cycles of the medium-carbon tests were stopped early to prevent the sample from brazing to the thermocouple. After reaching the maximum temperature, the furnace was turned off, and the samples were cooled in the protective atmosphere of the furnace chamber.

### C. Metallography

Upon cooling, samples were vacuum-cold mounted in epoxy and cross sectioned through the center. Each sample was prepared using the standard grinding and polishing procedure, to 0.3 μm with an alumina suspension. A Leica optical microscope was used to image the cross section of each sample. All samples were imaged in the unetched condition. Later, a 2 pct Nital solution was applied to medium-carbon substrates to reveal surface decarburization. Copper is easily distinguished from steel in optical microscopy. Scanning electron microscopy (Desktop Phenom G2 Pro, 5 kV working voltage in backscattered mode) was used to reveal the samples at higher resolution. Copper is distinguished as the lighter phase in these images. To determine the composition of the observed oxides and provide insight to the possible reactions resulting from the applied coatings, energy dispersive spectroscopy, EDS (Oxford instruments, x-act Penta FET Precision, 20 kV working voltage, IProbe = 50 pA) was performed at multiple points for several samples. To overcome difficulties with the nonconductive epoxy charging during EDS analysis, these samples were prepared with a gold coating and silver trace.

## III. RESULTS

Figure 3 shows snapshots of the copper droplet profiles on the low- and medium-carbon steel with different surface preparations at multiple temperatures upon melting, from 1060 °C to 1150 °C. The most obvious distinction is between the low- and medium-carbon substrates: the droplets on low-carbon steels are generally stable through to 1150 °C, while the droplet disperses and spreads, before the end of the heating cycle for the medium-carbon steels. The copper droplet on the coated low-carbon steels (with the exception of the oxidized- $\text{Na}_2\text{SO}_4$  sample) decreases in height and adopts an asymmetrical shape at the end of the thermal cycle. Amongst the various medium-carbon substrates, the droplet on the oxidized sample was stable for the longest, and shows the highest temperature reached before complete spreading across the substrate. The coatings on the medium-carbon substrates appear to accelerate wetting. The droplets on the  $\text{Na}_2\text{SO}_4$ -coated

medium-carbon samples show a textured, uneven surface developing on the droplet during spreading, while copper on the  $\text{Na}_2\text{SiO}_3$ -coated samples appears to flow rapidly under the lifted surface layer.

It should be noted that there is some variability on the left-hand side of the figure, in the temperature at which copper forms a droplet. Commercially available copper wiring was used. Oxygen is the main impurity present in electrical copper, typically in the range of 250 to 400 ppm. The copper-oxygen phase diagram shows this level of oxygen decreases the melting point by 10 °C to 15 °C. A discrepancy between the temperature of the sample and the temperature measured by the thermocouple is also present, which likely explains the different melting points observed between the tests. These factors should not affect the overall comparisons of droplet evolution between the different substrates.

Figure 4 quantifies the contact angle (averaged between the left- and right-hand sides of the droplet) for the low-carbon (a) and medium-carbon (b) substrates as temperature increases (at 5 °C/min). The star-shaped marker denotes when the droplet forms, and an x-shaped marker shows when an asymmetric shape evolves (defined as when the difference between the two sides is greater than 15 deg). Again, the main trend to note is the difference between the low- and medium-carbon substrates. The contact angle decreases to zero in all of the medium-carbon cases, with the oxidized medium-carbon substrate maintaining contact angle over 90 deg at the highest temperature. The droplets for the low-carbon cases show a slight, gradual decrease in contact angle. The  $\text{Na}_2\text{SiO}_3$  and  $\text{Na}_2\text{SO}_4$ -coated samples adopt an asymmetric shape at high temperature. The low-carbon sample treated in air shows the most rapid wetting behavior of all cases, never forming a spherical droplet, but spreading immediately over the surface.

The cross sections of the solidified copper on the substrates are compared side-by-side in Figure 5. The oxidized, ground, and as-received low-carbon steel samples show a spherical droplet with limited spreading. The reduced height and asymmetric shape of the droplets on the coated low-carbon samples is explained by some copper flow between the surface scale and the substrate. The exception is the oxidized- $\text{Na}_2\text{SO}_4$  sample, which shows no copper flow between the surface layer and the substrate and negligible diffusion of copper into the substrate. The medium-carbon substrates show copper spread sporadically over the top and bottom surfaces. In all cases, various pores, surface cracking and internal cavities of the copper droplet can be seen. This is a common observation for pure copper and high copper alloys, which are intrinsically susceptible to porosity.<sup>[35]</sup> The specific volume of copper decreases by 5 pct in the liquid–solid transition. Commercial copper casting uses a controlled, fine dispersion of oxygen to offset this decrease in volume. The sample cross sections exhibit cracks and pores from uncontrolled shrinkage and gas formation during solidification. Oxygen was present in liquid copper from the atmosphere and dissolution of the iron oxide. During cooling, oxygen solubility decreases. Excess oxygen can also react with hydrogen, resulting in water vapor porosity.<sup>[36]</sup>

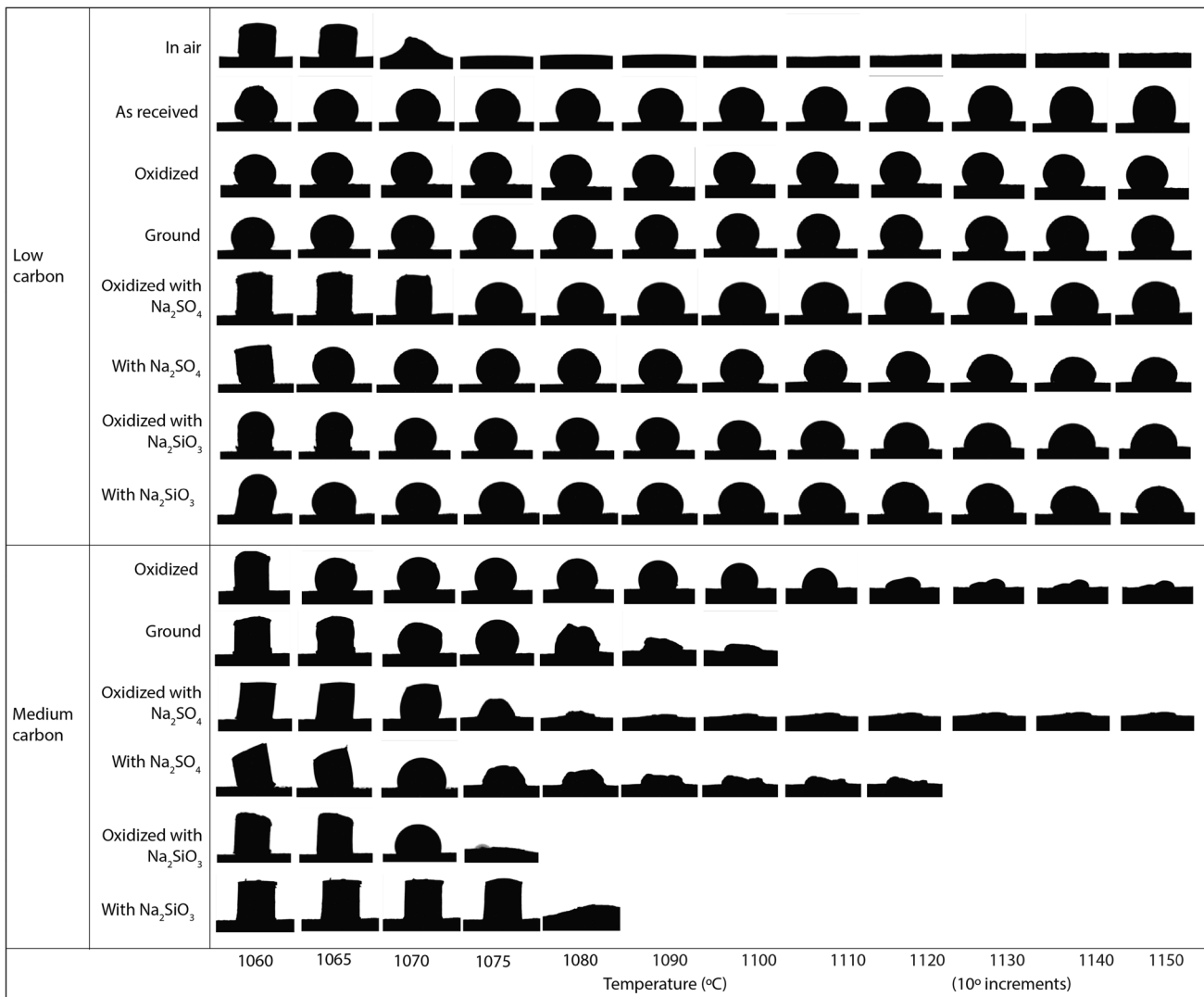


Fig. 3—Profiles of copper droplets on low-carbon and medium-carbon steels with different surface preparations from 1060 °C to 1080 °C at 5 °C increments and 1080 °C to 1150 °C at 10 °C increments.

#### IV. DISCUSSION

The mechanisms controlling the observed wetting behavior must be determined. As discussed in the introduction, diffusion of liquid copper into the steel substrate, as well as chemical dissolution, reduction, and mechanical disruption of the oxide are known to promote wetting of copper to steel. Examining the varied substrates at higher magnification reveals evidence of these mechanisms. The implications for process development are then discussed.

##### A. Liquid Copper Wetting on Steel in Air

Figure 6 shows how copper distributes within the typical three-oxide-layered scale that forms on low-carbon steel when air is circulated through the furnace. The majority of the scale would be wüstite at high temperature, which transforms partially to magnetite upon cooling. Copper penetrates the pores in the wüstite, while the majority of copper appears to be present at a

seam close to the substrate. This seam exhibits nonuniform features of oxides and pores. It appears iron oxide was delaminated from the surface by the flowing liquid copper, which exposed the surface to oxygen to allow further reaction. This result confirms that to enable copper separation, scale formation must be limited.

##### B. Liquid Copper Wetting on Low-Carbon Substrates

Figure 7 shows micrographs of the main features of the copper droplets on the as-received and initially ground and oxidized low-carbon substrates. The main phenomena shown in these images are iron oxide dissolution and oxide precipitation within and on the surface of the copper droplet, copper diffusion into the substrate, and liquid copper flowing outwards in the gap between the oxide scale and substrate. The initially oxidized sample shows more oxide dissolution (and iron oxide precipitation) than the initially ground sample. EDS analysis reveals that iron oxide precipitated as a

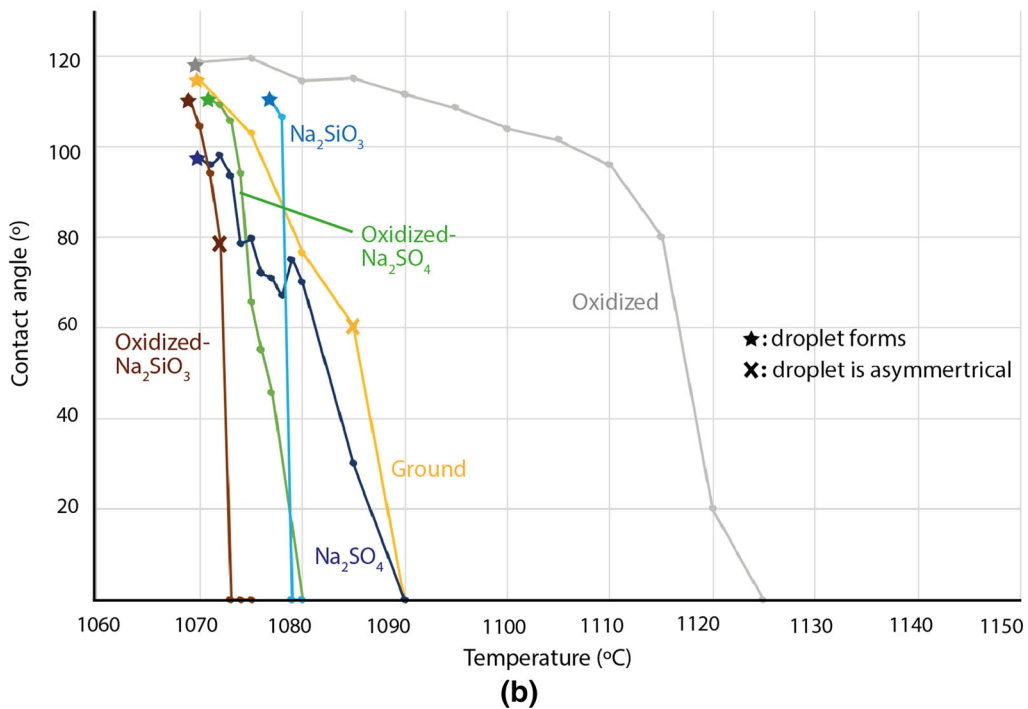
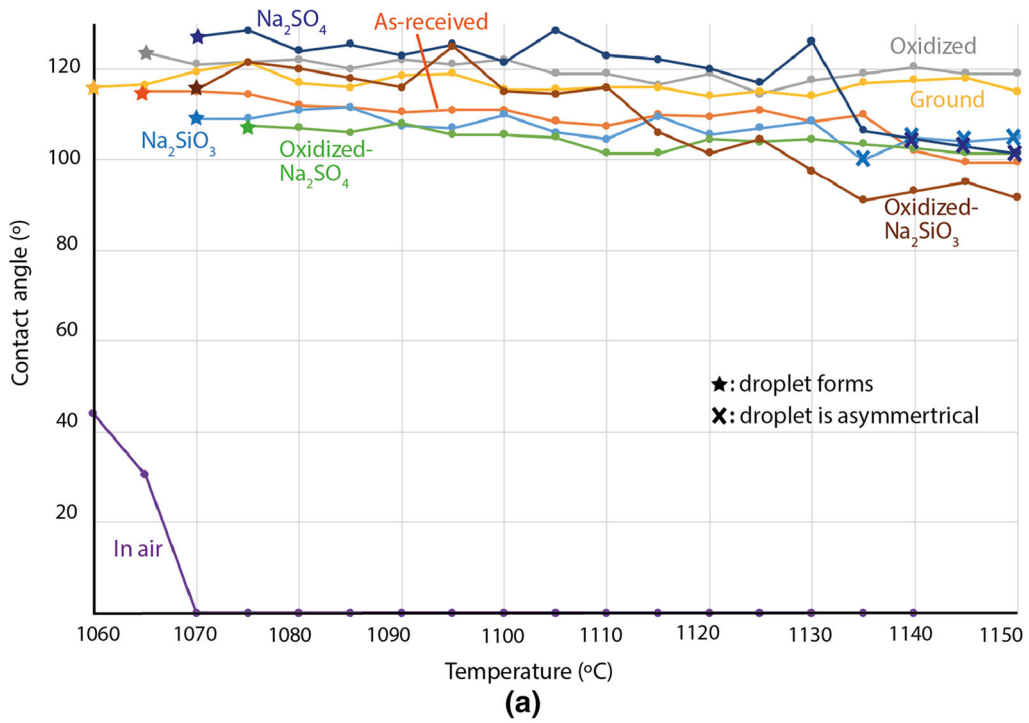


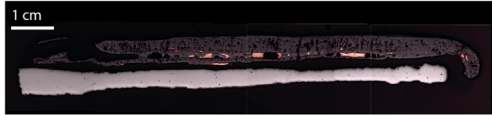
Fig. 4—Droplet contact angle over temperature for the various preparations of low-carbon substrates (a) and medium-carbon substrates (b). The heating rate in all cases is 5 °C/min.

seam in the copper droplet. A thin oxide formed on the surface of the copper droplet (EDS analysis shows the composition of this oxide varies and contains both iron and copper). For all samples, the iron oxide scale shows two layers distinguishable by color. The surface layer is a higher-oxygen oxide, magnetite or hematite. When contact of the scale with the substrate is disrupted, the

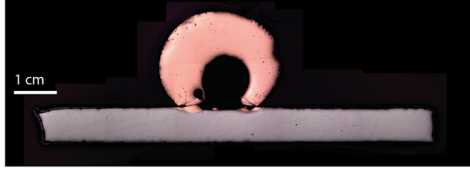
transport of Fe ions is disrupted as well and the scale oxidizes further. The transformation of the iron oxide scale after a gap forms between the scale and substrate is described by Kim and Lee.<sup>[37]</sup> Thus, the proportion of the higher-oxygen oxide layer is an indication of when the scale was disrupted. The flow of liquid copper disrupted scale contact, especially for the as-received

**Low carbon**

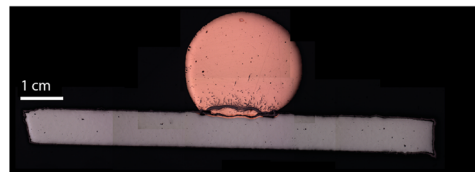
In air



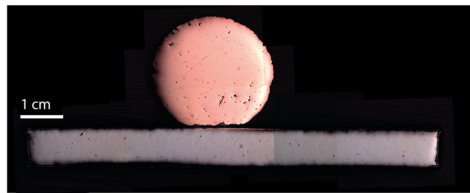
As received



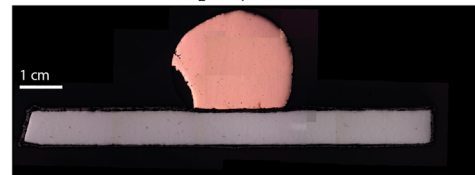
Oxidized



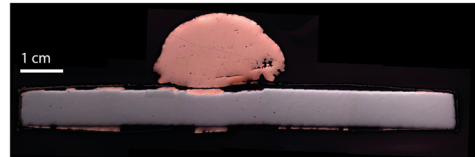
Ground



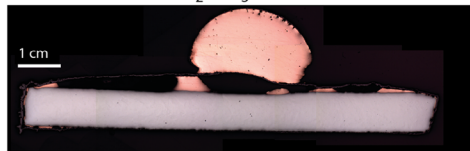
Oxidized with  $\text{Na}_2\text{SO}_4$



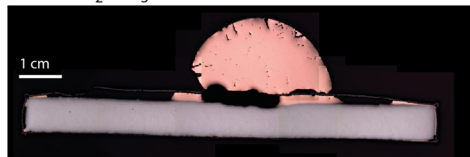
With  $\text{Na}_2\text{SO}_4$



Oxidized with  $\text{Na}_2\text{SiO}_3$

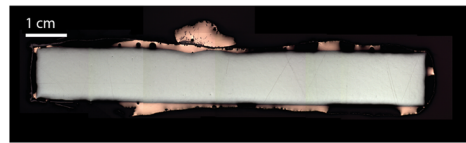


With  $\text{Na}_2\text{SiO}_3$

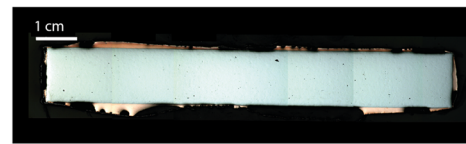


**Medium carbon** Maximum T reached (°C)

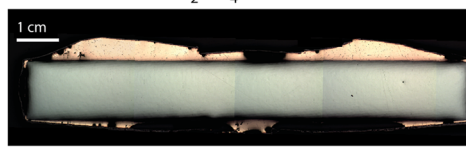
Oxidized 1150



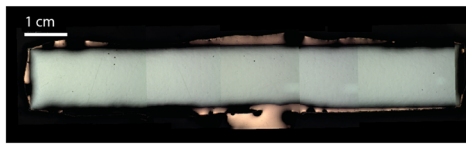
Ground 1108



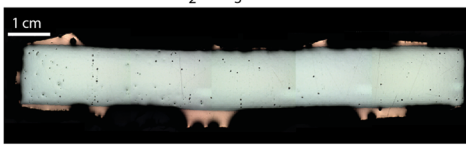
Oxidized with  $\text{Na}_2\text{SO}_4$  1150



With  $\text{Na}_2\text{SO}_4$  1115



Oxidized with  $\text{Na}_2\text{SiO}_3$  1076



With  $\text{Na}_2\text{SiO}_3$  1081



Fig. 5—Cross sections of solidified copper on all substrate preparations. All samples were cooled in the furnace chamber after the thermal cycle. All low-carbon samples reached a maximum temperature of 1150 °C, but to prevent brazing of liquid copper to the alumina sheaths, the thermal cycle was stopped early for most medium-carbon samples. The maximum temperature reached for the medium-carbon samples is shown in the figure.



and ground conditions. Copper wets to the iron substrate beneath the surface scale, but overall a stable droplet with limited outward copper flow between the oxide layer and substrate can be achieved on uncoated low-carbon steel whether there is a significant oxide layer initially present, or if the surface is ground or

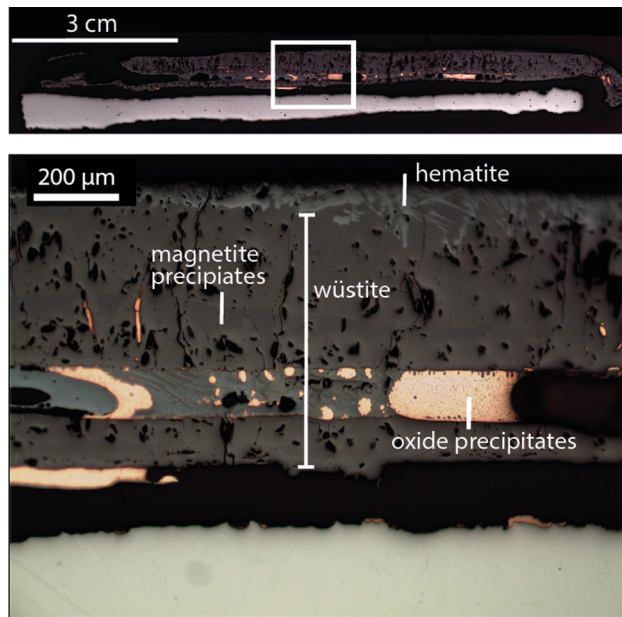


Fig. 6—Iron oxide scale with liquid copper entrapment when low-carbon steel was treated in air.

in the as-received condition. The oxygen in the furnace atmosphere reacts to form an adherent iron oxide layer on the initially ground sample. The oxygen also increases the surface tension of liquid copper and reacts to form surface oxides to impede droplet flow.

Figure 8 shows the low-carbon samples with an applied  $\text{Na}_2\text{SO}_4$  coating. There is a significant difference in wetting behavior between the  $\text{Na}_2\text{SO}_4$ -coated initially oxidized and ground samples. Decohesion of the oxide with the substrate is observed in the initially ground sample, with copper flowing in this gap, while the scale on the oxidized- $\text{Na}_2\text{SO}_4$  sample appears to be the most resistant against disruption from the liquid copper. The difference between the two samples may be the reaction progression.  $\text{Na}_2\text{SO}_4$  deposits on iron at high temperature cause an accelerated oxidation reaction known as “hot corrosion.” Iron reacts with  $\text{Na}_2\text{SO}_4$  to form iron sulfide and oxides. Shi<sup>[38]</sup> shows that  $\text{Na}_2\text{SO}_4$ - $\text{Na}_2\text{O}$  eutectic melt is formed, which maintains contact between the  $\text{Na}_2\text{SO}_4$  deposit and substrate to progress the reaction. Iron oxide dissolves in the melt and precipitates as discrete particles at the melt/solid interface. Once all the sulfate ions are reduced, only solid  $\text{Na}_2\text{O}$  and iron oxide are left. EDS analysis confirms that the scale of the  $\text{Na}_2\text{SO}_4$ -coated initially oxidized sample consists of iron oxide at all points tested. With significant iron oxide initially present, the reaction may have progressed to completion, such that the scale was solid and protective when the liquid copper melted. However, hot corrosion may have been in the propagation stage for the initially ground sample. The molten deposit destroys the protective reaction-product oxide

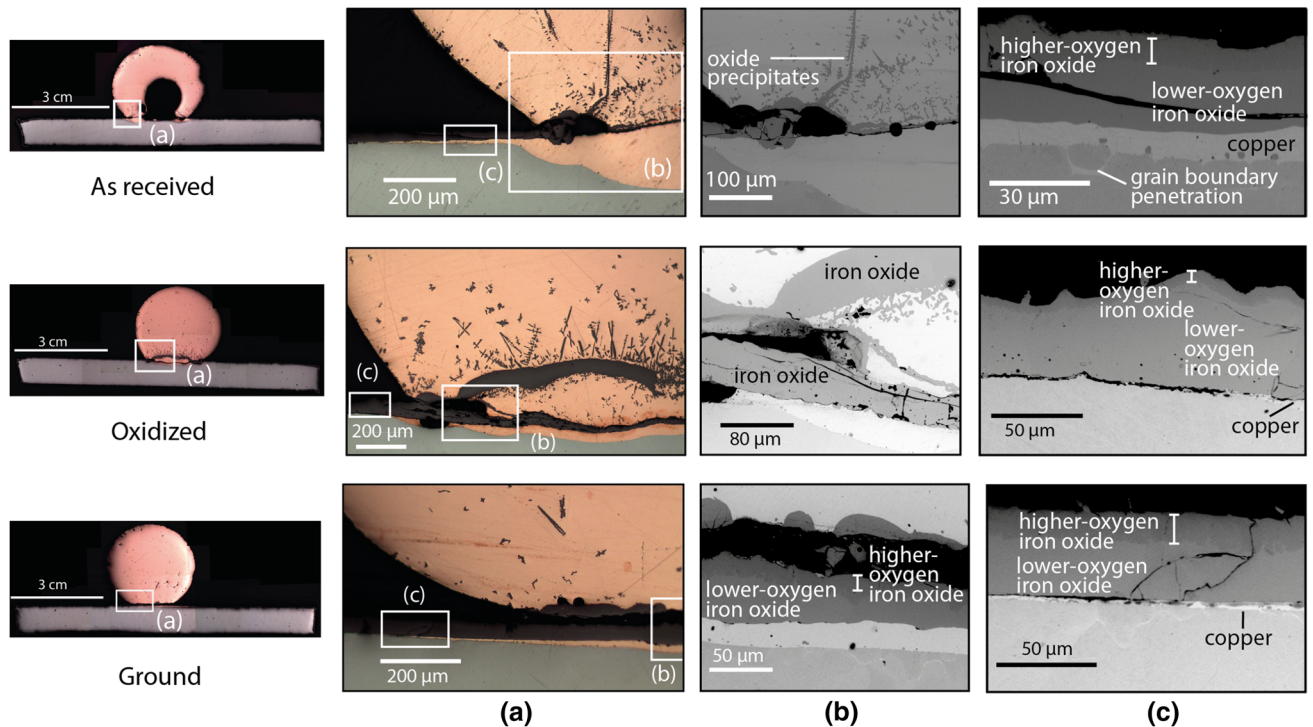


Fig. 7—Optical micrographs of the copper droplet on low-carbon steel substrates in the as-received, oxidized, and initially ground conditions (a). SEM images in (b) show the copper/oxide/steel interface. SEM images of the oxide layer are shown in (c).

scale,<sup>[39]</sup> and the scale may have fractured at the molten layer, a weak point. Overall, it appears that attaining a resilient, nonwetting scale with the  $\text{Na}_2\text{SO}_4$  deposit depends on the initial oxidation condition. If the reaction is incomplete, the deposit may weaken the scale with a liquid reaction product.

The cross sections of the initially ground and oxidized surfaces coated with  $\text{Na}_2\text{SiO}_3$  are shown in Figure 9. The coating appears to have caused decohesion between the iron oxide and steel substrate, which then provided a pathway for copper flow.  $\text{Na}_2\text{SiO}_3$ , also known as waterglass, is used in a wide range of high-temperature adhesion and repair applications. The melting point of  $\text{Na}_2\text{SiO}_3$  is 1089 °C.<sup>[40]</sup> During heating, excess water evaporates such that waterglass cures<sup>[41]</sup> in a polymerization process,<sup>[42]</sup> leaving silicate compounds with glass-like properties. The material can flow to fill cracks and act as a sealant. In this case, it appears the applied  $\text{Na}_2\text{SiO}_3$  flowed through the oxide layer and the silicate

compounds collected in the wüstite pores, shown as the darker phase at the base of the oxide scale. EDS analysis confirms that the scale consists of iron oxide and another phase, in which Na, Si and O present, but could not be stoichiometrically identified.  $\text{SiO}_2$  may have reacted with iron oxide and form fayalite,  $\text{Fe}_2\text{SiO}_4$ . Surface roughness at the interface is also evident, a feature of fayalite formation.<sup>[43]</sup> Overall, the formation of a silicon-rich liquid phase may have compromised the connection between the oxide layer and the substrate, allowing copper flow. Silicates may have also introduced additional stress and volume mismatch between the oxide and substrate. Lastly, the vaporization of water may have also contributed to the lack of adhesion. Matsumoto *et al.*<sup>[44]</sup> studied the adhesive performance of waterglass and found the adhered film thickness decreased as temperature increased up to 1000 °C, which the authors attributed to the formation of a vapor film. In any case,  $\text{Na}_2\text{SiO}_3$  did not act to seal the

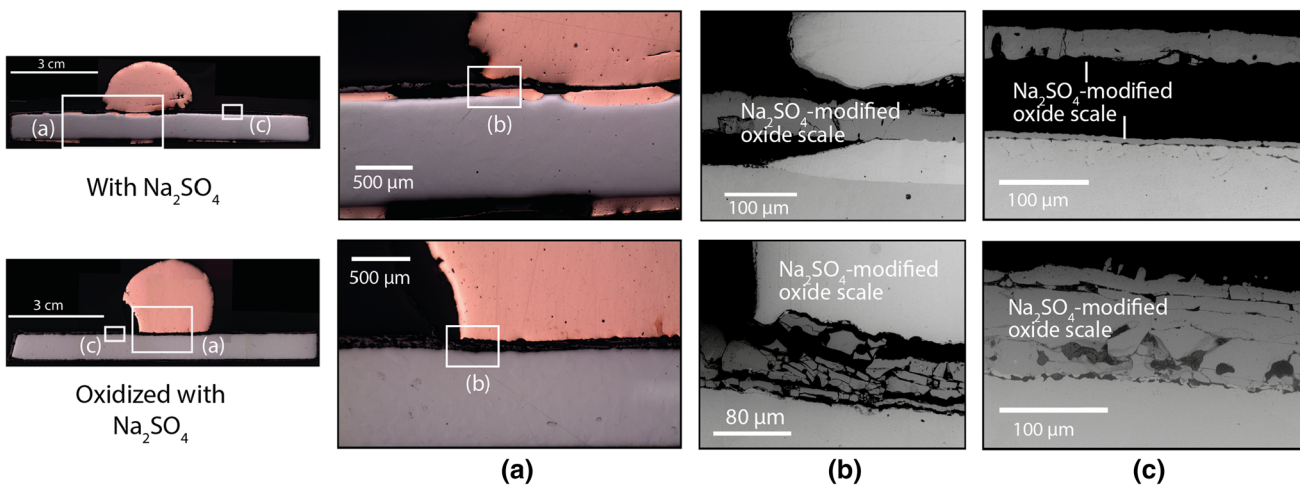


Fig. 8—Optical micrographs of the copper droplet on initially ground and initially oxidized low-carbon steel substrates with an applied  $\text{Na}_2\text{SO}_4$  coating (a). SEM images in (b) show the copper/oxide/steel interface. SEM images of the oxide layer are shown in (c).

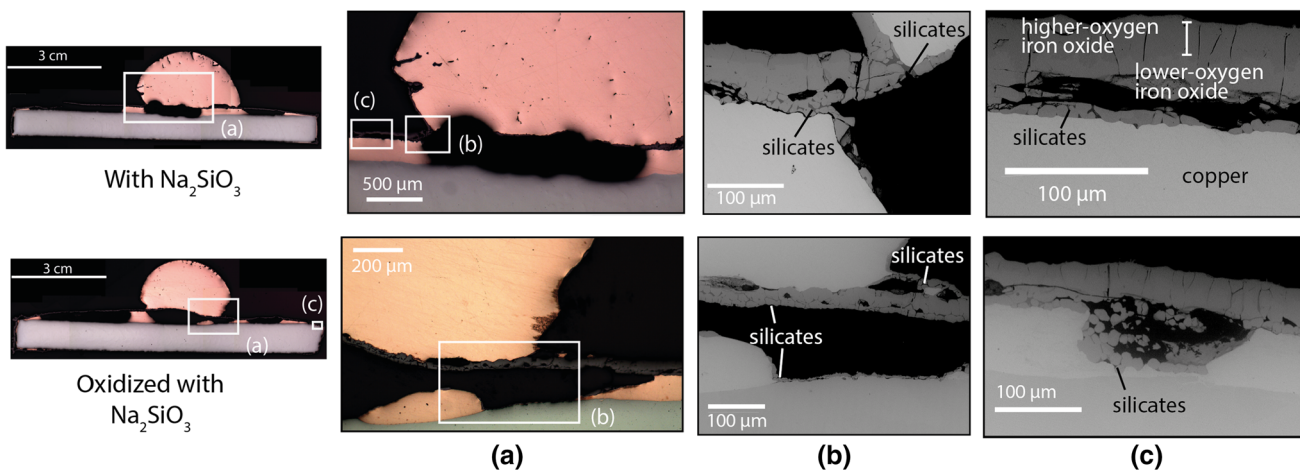


Fig. 9—Optical micrographs of the copper droplet on initially ground and initially oxidized low-carbon steel substrates with an applied  $\text{Na}_2\text{SiO}_3$  coating (a). SEM images in (b) show the copper/oxide/steel interface. SEM images of the oxide layer are shown in (c).

connection between the oxides in substrate. The mechanisms of iron oxide dissolution and copper oxide precipitation at the base of the droplet are not apparent.

### C. Liquid Copper Wetting on Medium-Carbon Substrates

The images revealing the main characteristics of the medium carbon initially ground and initially oxidized cross sections are shown in Figure 10. Copper established a connection with the steel substrate and penetrated grain boundaries by flowing between the oxide layer and substrate. The oxidized sample exhibited the slowest spreading of all the medium-carbon substrates, and evidence of iron oxide dissolution in copper and precipitation of a seam of iron oxide, similar to the low-carbon cases, can be seen. The spread of copper is sporadic, and pores and formation of an oxide on the surface of copper can be seen. The oxidation of the liquid copper surface during spreading may have contributed to the sporadic distribution, as copper oxide would act to intervene and prevent liquid flow. The iron oxide scale on the uncoated medium-carbon samples is much thinner than the oxide scale observed in the uncoated low-carbon samples.

The extensive wetting in the medium-carbon cases cannot be attributed only to the lack of adherence between the oxide and substrate, as decohesion was observed for coated low-carbon substrates, but the droplet remained intact. It is likely that the formation of CO(g) caused bulging and blistering of the scale to accelerate wetting. As reviewed by Chen *et al.*,<sup>[45]</sup> all steel types are susceptible to blistering above 800 °C due to internal stresses during growth as iron ions diffuse outward and vacancies diffuse inward, as well as from the differing crystal structures and thermal expansion coefficients between the scale and substrate. However,

higher-carbon steels are more susceptible to blistering due to the accumulation of gases. Carbon reacts with oxygen in wüstite to form CO(g), which fills pores and voids in the scale, or escapes through cracks and ruptures. CO(g) can also act as an additional reductant to produce CO<sub>2</sub>(g). Figure 11 shows the initially oxidized medium-carbon sample upon etching with Nital to reveal ferrite ( $\alpha$ -Fe, the white phase) and cementite (Fe<sub>3</sub>C, the dark phase). The decreased presence of cementite close to the surface confirms significant decarburization. The etched original medium-carbon steel material is shown in image (c) for comparison.

The scale on the medium-carbon steel also appears to be intrinsically more irregular and less adherent. Figure 12 shows the initial oxide scales at several points formed on the low- and medium-carbon steels after the oxidizing treatment, before testing. The oxide scale on low-carbon steel was thick and adherent, while the scale on the medium-carbon steel was thinner, and in places detached or exhibited pores at the interface. Carbon is known to cause a more erratic oxidation reaction,<sup>[46]</sup> but the steels also had different processing histories. Medium-carbon steels are typically in the form of bars, and may be hot rolled or annealed. Low-carbon steels are more commonly cold-rolled into sheets. More adherent and thicker scales form on cold-worked surfaces, while the scale adhesion on annealed/electropolished surface is poor, resulting in an irregular scale structure.<sup>[47]</sup>

The cross sections of the medium-carbon substrates with the Na<sub>2</sub>SO<sub>4</sub> coating are shown in Figure 13. It appears that the reaction for a solid, protective scale was incomplete for the Na<sub>2</sub>SO<sub>4</sub>-coated samples. The blistering of the scale would have disrupted contact between the substrate and Na<sub>2</sub>SO<sub>4</sub> coating to terminate the hot corrosion reaction. EDS analysis shows that the majority of the scale is iron oxide, but an occluded darker

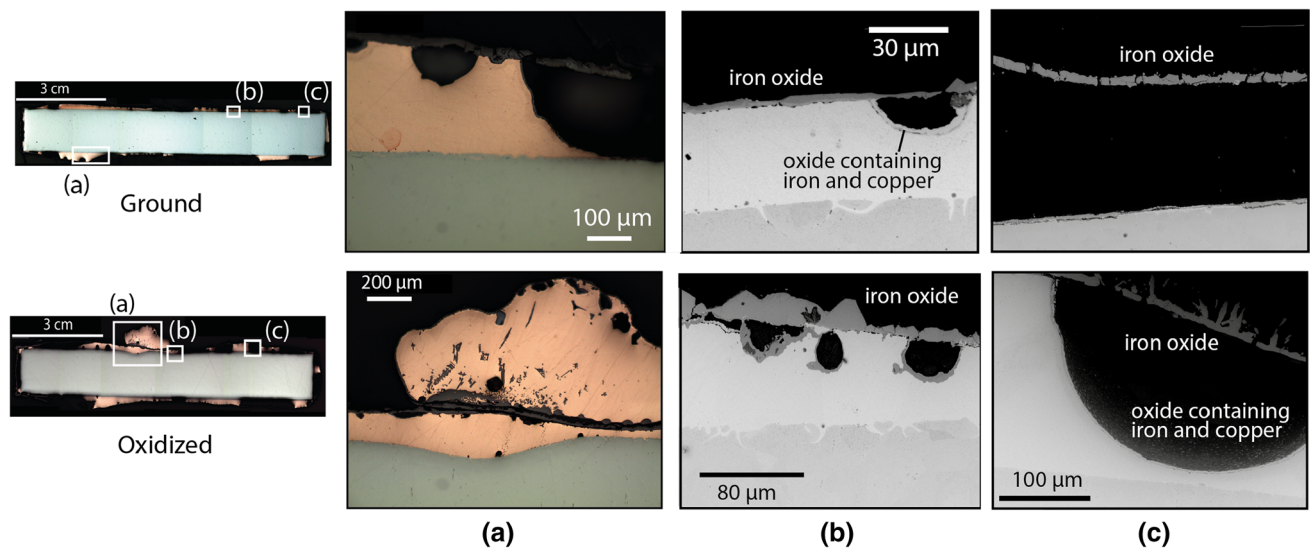


Fig. 10—Optical micrographs of the copper spread on medium-carbon steel substrates in the initially ground and initially oxidized condition (a). SEM images in (b) show the copper/oxide/steel interface. SEM images of the oxide layer are shown in (c).

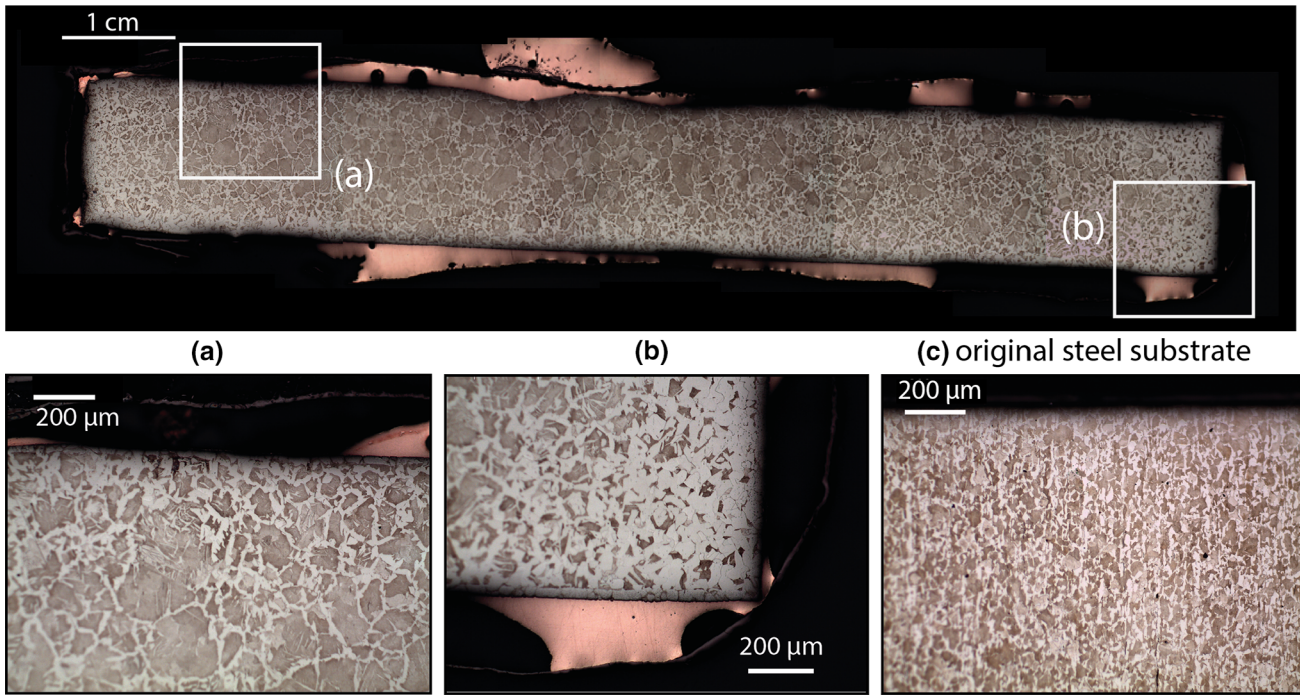


Fig. 11—The initially oxidized medium-carbon substrate with a 2 pct Nital etching to reveal decarburization, with higher magnification images shown in (a) and (b). The etched original medium-carbon substrate is shown in image (c).

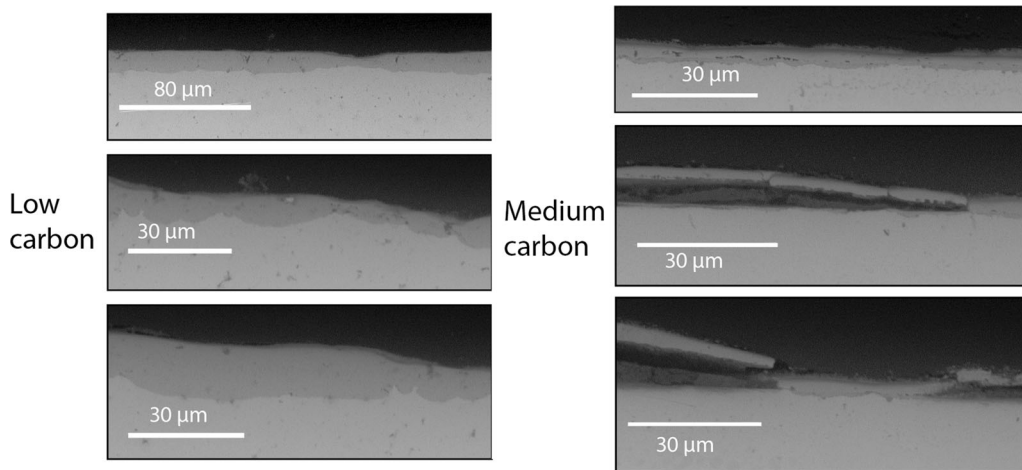
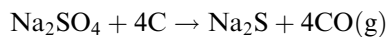
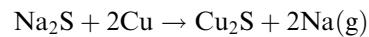


Fig. 12—Initial oxide scales for medium- and low-carbon steel samples.

phase contains significant quantities of Fe, Na, O, as well as Si (which would have oxidized from the Si-containing steel substrate and may have formed fayalite). It appears that  $\text{Na}_2\text{SO}_4$  and  $\text{Na}_2\text{S}$  may have reacted with copper upon melting. Voids in the scale close to the interface are apparent. Carbon from the steel, or  $\text{CO}(\text{g})$ , may have reduced the  $\text{Na}_2\text{SO}_4$  deposit to form  $\text{Na}_2\text{S}$  and  $\text{CO}(\text{g})$  or  $\text{CO}_2(\text{g})$ , respectively.



The reaction of copper with  $\text{Na}_2\text{S}$ , shown below, is well known to be favorable.<sup>[48]</sup> Precipitates are distributed throughout the solidified copper, which EDS analysis confirms is copper sulfide.



The droplet profiles of the medium-carbon  $\text{Na}_2\text{SO}_4$ -coated samples in Figure 3 show a textured reaction product enveloping the surface of the copper droplet as it spreads.

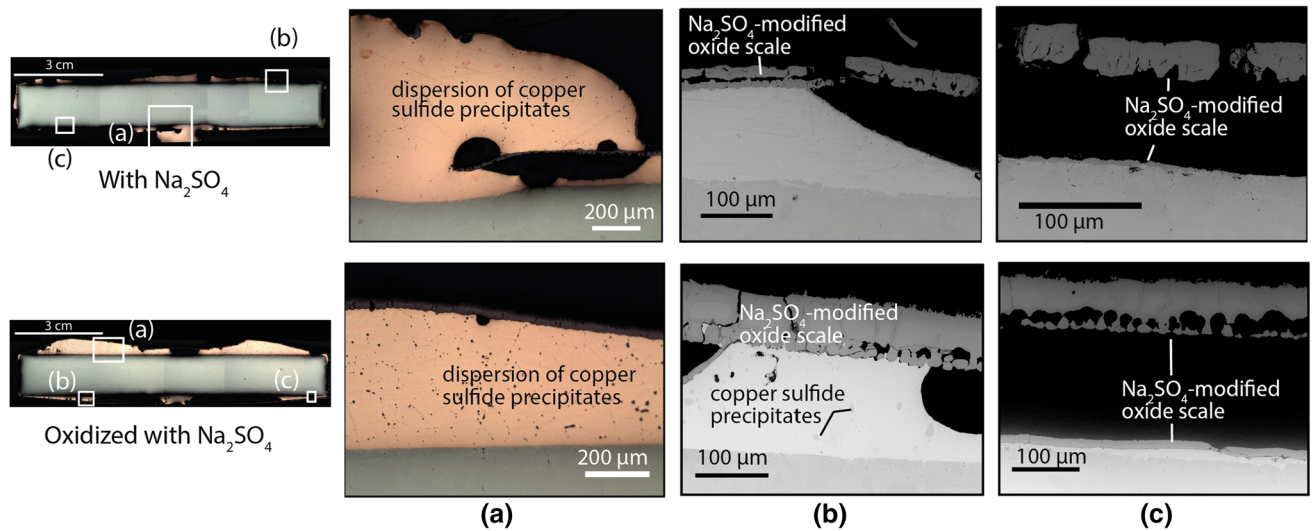


Fig. 13—Optical micrographs of the copper spread on medium-carbon steel substrates in the initially ground and initially oxidized condition with the  $\text{Na}_2\text{SO}_4$  coating applied (a). SEM images in (b) show the copper/oxide/steel interface. SEM images of the oxide layer are shown in (c).

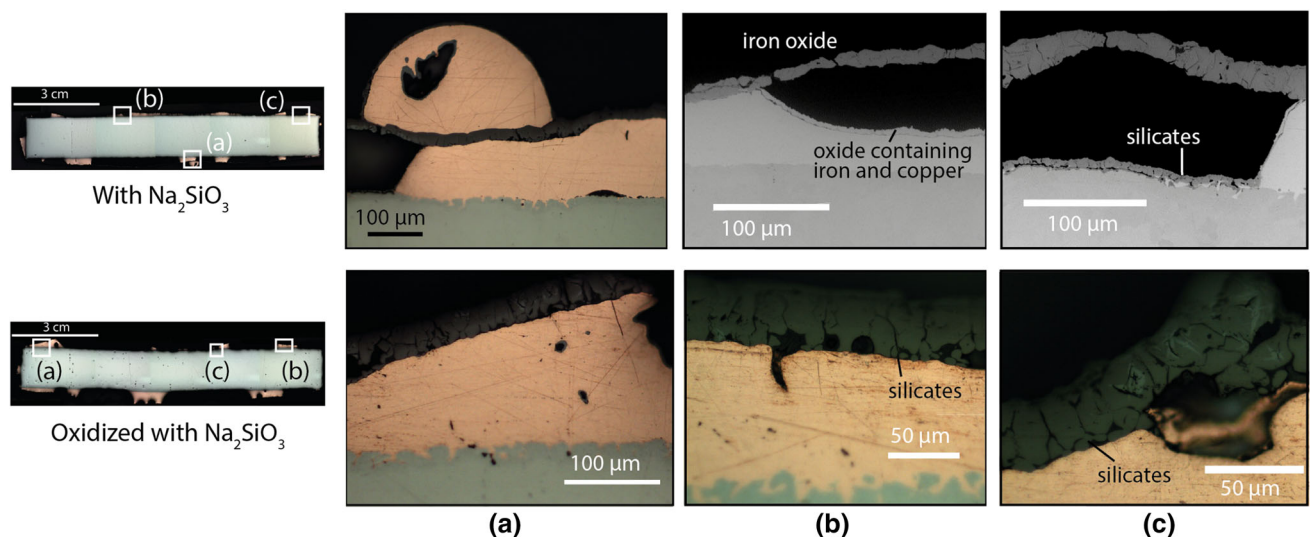


Fig. 14—Optical micrographs of the copper spread on medium-carbon steel substrates in the initially ground and initially oxidized condition with the  $\text{Na}_2\text{SiO}_3$  coating applied (a). SEM images in (b) show the copper/oxide/steel interface. SEM (optical for the oxidized with  $\text{Na}_2\text{SiO}_3$  sample due to issues with sample preparation) images of the oxide layer are shown in (c).

Figure 14 shows the features of the  $\text{Na}_2\text{SiO}_3$  coated samples. Again, it appears silicates are present as a darker phase in the oxide, but this likely aided in decohesion. It appears the scale lifted and provided a pathway for copper flow. The spreading of liquid copper was most rapid for  $\text{Na}_2\text{SiO}_3$ -coated medium-carbon samples.

Overall, the coatings do not appear to be especially useful. The improved liquation aided by  $\text{Na}_2\text{SO}_4$  and  $\text{Na}_2\text{SiO}_3$  as described by Leak and Fine<sup>[26,28]</sup> is not substantiated here. The difference in environments between this study and the study by Leak and Fine may explain this discrepancy. The molten salts employed in their tests,  $\text{BaCl}_2$  and  $\text{CaCl}_2$ , may have dissolved the iron oxide scale present, such that the

$\text{Na}_2\text{SO}_4$  and  $\text{Na}_2\text{SiO}_3$  barriers were critical to prevent brazing. In a gaseous environment, the coatings weaken adherence between the scale and substrate to provide a pathway for copper flow.

#### D. Process Development

These results provide a basis to begin defining a preferential melting process. As discussed in the introduction, copper external to steel requires less energy to remove compared to copper dilute in the steel melt. Upon melting steel scrap, copper and iron are completely miscible, but the solubility of liquid copper in solid austenite is limited. Indeed, the limited solubility of liquid copper in austenite as iron oxidizes during hot

rolling is the principle behind the surface hot shortness problem. The proposed preferential melting process seeks to exploit the same principle, but during scrap heating. Wetting must be minimized, so an adherent nonmetallic surface layer must be maintained for the duration of the treatment. Copper may wet to the steel substrate once the surface layer is penetrated or compromised, but the results here show a stable liquid copper droplet can be achieved on an uncoated low-carbon steel in an inert, or lightly oxidizing, atmosphere. Further work required to develop this idea is discussed below. Directions for exploring a wider range of conditions are discussed as well.

For energy-efficiency and industrial feasibility, the heat for preferentially melting copper must be retained to then melt the steel scrap, so the process conditions must be compatible with the conventional EAF route. The conditions of low-carbon content and a lightly oxidizing atmosphere to achieve nonwetting do not present any significant scale-up obstacles. However, further work is required to determine the levels of carbon concentration and oxygen partial pressure, which cause liquid copper to transition from nonwetting to wetting behavior. Low-carbon sheet steel is used in cars, goods, and equipment, which makes up the shredded scrap contaminated by copper. However, these steels may contain up to 0.25 wt pct C. Decarburization can be prevented by adjusting the furnace atmosphere, specifically by increasing the carbon potential. The atmospheric conditions required to heat treat a range of carbon steels while avoiding decarburization are specified,<sup>[31,34]</sup> so knowledge and expertise in downstream processing could be applied to scrap heating. Similarly, the oxygen potential of the atmosphere must be further investigated to determine the boundary between achieving a protective, thin oxide layer on both the droplet and substrate, and problematic entrapment of liquid in the scale.

Knowledge on scaling behavior during steel cooling and hot rolling could be applied. Scale formation and adhesion has been studied extensively.<sup>[49]</sup> Increased H<sub>2</sub>O or CO<sub>2</sub> in the atmosphere is known to increase the plasticity of the scale and improve adhesion.<sup>[45]</sup> Precipitating a magnetite seam at the scale/steel interface with an appropriate heating profile is also shown to improve adhesion,<sup>[50]</sup> and there are many coatings to control the iron scale proposed in patents.<sup>[51,52]</sup>

The other key part of the process is applying a mechanical force to separate liquid copper from the steel surface. Dynamic flow behavior of a liquid metal on a solid substrate can generally be inferred from the evolution of a static droplet.<sup>[22]</sup> However, the goal of the process would be to minimize contact and avoid phenomena such as dissolution of the oxide layer and penetration into pores observed in these static tests. The time-scale of these behaviors and how liquid copper flows over the scale must be determined with further experimental testing.

A liquid environment, such as a chemically inert molten salt bath, might be especially helpful to aid in the separation of liquid copper from steel. The bath composition could be optimized to promote coalescence

of the liquid copper, increase the thermal efficiency of heating, and decrease the weight of the scrap by 25 to 60 pct due to buoyancy,<sup>[53]</sup> which would help with shaking and agitation. The salt bath could also aid in controlling substances covering end-of-life steel scrap such as, zinc, paints, and tin coatings. The combustion of these substances during current EAF steelmaking is problematic, causing dust and pollution,<sup>[54]</sup> and alternative processes for preheating scrap while simultaneously removing or treating coatings are being developed.<sup>[55,56]</sup> Molten salt baths are currently investigated at the pilot scale as a more efficient and clean method to treat municipal waste.<sup>[57]</sup> Such setups are scalable, as molten salts are also widely used in metallurgy, for aluminum melting and steel heat treating. The interaction of liquid copper with the steel surface in an inert molten salt must be explored.

Thus, future study is required to investigate promising directions for process development. Overall, a viable process must be designed through an iterative consideration of scientific and practical aspects: converging an understanding of the wetting behavior of copper on steel, with the industrial constraints of treating heterogeneous end-of-life scrap.

## V. CONCLUSIONS

This study establishes the influence of steel carbon content, initial surface oxidation, and coatings on the wetting behavior of liquid copper to steel. The key parameter to affect rapid wetting appears to be carbon content. Blistering of the oxide scale provided a pathway for extensive copper flow between the scale and substrate. The Na<sub>2</sub>SO<sub>4</sub> and Na<sub>2</sub>SiO<sub>3</sub> coatings appeared to weaken the connection between iron and its oxide to allow copper flow, to supersede the typical iron oxide dissolution observed in the noncoated samples. The exception was the oxidized-Na<sub>2</sub>SO<sub>4</sub> surface on low-carbon steel—the resultant scale was fully intact at the interface and prevented liquid copper penetration. The applicability of the coatings is questionable, but a stable droplet was observed on the uncoated low-carbon steel regardless of the initial oxidation condition, which is promising for future process development. With a renewed urgency to control copper in steel recycling, previously investigated techniques must be reconsidered. For this technique and others, it is important to test the limits for controlling tramp elements.

## ACKNOWLEDGMENTS

K.D. is funded by a Cambridge Trust scholarship. A.S. and J.A. are funded by EPSRC, grant reference EP/N02351X/1. The authors are grateful to the Materials Processing Institute (MPI), for providing equipment and training for the sessile drop experiments. Len Howlett at the University of Cambridge provided essential help with initial experimental ideas, sample preparation, and microscopy, and Graham Smith assisted with EDS analysis.

## OPEN ACCESS

This article is distributed under the terms of the Creative Commons Attribution 4.0 International License (<http://creativecommons.org/licenses/by/4.0/>), which permits unrestricted use, distribution, and reproduction in any medium, provided you give appropriate credit to the original author(s) and the source, provide a link to the Creative Commons license, and indicate if changes were made.

## REFERENCES

1. L. Savov, E. Volkova, and D. Janke: *Mater. Geoenviron.*, 2003, vol. 50, pp. 627–40.
2. B. Björkman and C. Samuelsson: in *Handbook of Recycling*, ed. E. Worrell and M. Reuter, Elsevier, Oxford, 2013, pp. 65–83.
3. O. Rod, C. Becker, and M. Nylén: *Jernkontoret Rep.*, 2006, pp. 1–59.
4. M. Huellen, C. Schrade, U. Wilhelm, and Z. Zulhan: *Ironmak. Steelmak. Conference*, 2006, paper 7.1.
5. K. Daehn, A. Serrenho, and J. Allwood: *Environ. Sci Technol.*, 2017, vol. 51, pp. 6599–6606.
6. K.E. Daehn, A.C. Serrenho, and J. Allwood: *Metall. Mater. Trans. B*, 2019. <https://doi.org/10.1007/s11663-019-01537-9>.
7. A. Cohen and M. Blander: *Metall. Mater. Trans. B.*, 1998, vol. 29B, pp. 493–95.
8. L. Savov and D. Janke: *ISIJ Int.*, 2000, vol. 40, pp. 95–104.
9. S. Newell: *International Conference on Recycling in the Iron and Steel Industry*, October 1996.
10. M. Shattuck and C. Ramsdell: The case for producing low-copper steel with ballistic separators (Waste Advantage, 2018) <https://wasteadvantagemag.com/the-case-for-producing-low-copper-steel-with-ballistic-separators/>. Accessed January 2019.
11. E.A. Brandes and G.B. Brook: *Smithells Metals Reference Book*, 7th ed., Butterworth-Heinemann, Oxford, 1992.
12. C.P. Manning and R.J. Fruehan: *JOM*, 2001, vol. 53, pp. 36–43.
13. H. Katayama, N. Sano, M. Sasabe, and S. Matsuoka: *Iron and Steel—Today, Yesterday, and Tomorrow Research Conference Proceedings*, 1997, vol. 1, pp. 15–26.
14. L. Froschauer and R.M. Fulrath: *J. Mater. Sci.*, 1975, vol. 10, pp. 2146–55.
15. H. Fredriksson, K. Hansson, and A. Olsson: *Scand. J. Metall.*, 2001, vol. 30, pp. 41–50.
16. N. Eustathopoulos, M.G. Nicholas, and B. Drevet: *Wettability at High Temperatures*, vol. 3, Elsevier, Amsterdam, 1999.
17. R.R. Brown and F.E. Block: U.S. Bureau of Mines, Report 7218, 1968.
18. W. Schwenk and A. Rahmel: *Oxid. Met.*, 1986, vol. 25, pp. 293–303.
19. S. Hara: *ISIJ*, 1996, p. 105.
20. E. Bernardo, R. Oro, M. Campos, and J.M. Torralba: *Adv. Powder Technol.*, 2016, vol. 27, pp. 1027–35.
21. N. Takahira, T. Tanaka, S. Hara, and J. Lee: *Mater. Trans.*, 2005, vol. 46, pp. 3008–14.
22. N. Eustathopoulos and B. Drevet: *J. Phys. III*, 1994, vol. 4, pp. 1865–81.
23. P. Protsenko and N. Eustathopoulos: *J. Mater. Sci.*, 2005, vol. 40, pp. 2383–87.
24. P. Shen, Y. Gu, NN Yang, RP Zheng, and LH Ren: *Appl. Surf. Sci.*, 2015, vol. 328 (1), pp. 380–86.
25. B. Komolafe and M. Medraj: *J. Metall.*, 2014, vol. 2014, Article ID 387046.
26. V.G. Leak, M.M. Fine, and H. Dolezal: U.S. Bureau of Mines, Report 7809, 1973.
27. H.R. Nelson: *J. Chem. Phys.*, 1937, vol. 5, pp. 252–59.
28. V.G. Leak and M. Fine: U.S. Patent 3,776,718, 1973.
29. B. Gallois and CHP Lupis: *Metall. Trans. B*, 1981, vol. 12B, pp. 549–57.
30. T. Young: *Philos. Trans. R. Soc. Lond.*, 1805, vol. 95, pp. 65–87.
31. D.H. Herring: *Industrial Heating.com*, October 2009, pp. 45–48.
32. H.F. Marston, P.H. Bolt, G. Leprince, M. Röder, R. Klima, J. Niska, and M. Jarl: *Ironmak. Steelmak.*, 2004, vol. 31, pp. 57–65.
33. J.R. Arthur: *Trans. Faraday Soc.*, 1951, vol. 47, pp. 164–78.
34. Furnace Atmospheres No. 2 Neutral Hardening and Annealing (Linde Gas) [https://www.linde-gas.com/en/legacy/attachment?file\\_s=tcm:lg.17-460205,tcm:17-460205,tcm:17-460205](https://www.linde-gas.com/en/legacy/attachment?file_s=tcm:lg.17-460205,tcm:17-460205,tcm:17-460205). Accessed March 2019.
35. R. Konečná, and S. Fintová: *InTech*, 2012.
36. Volume Deficits of Castings Made from Copper and Copper Alloys (BDG, 2010) [https://www.bdguss.de/fileadmin/content\\_bdguss/Der\\_BDG/Richtlinien/P\\_211en.pdf](https://www.bdguss.de/fileadmin/content_bdguss/Der_BDG/Richtlinien/P_211en.pdf). Accessed March 2019.
37. S. Kim and H. Lee: *Steel Res. Int.*, 2009, vol. 80, pp. 121–29.
38. L. Shi: *Oxid. Met.*, 1993, vol. 40, pp. 197–211.
39. N. Birks, G.H. Meier, and F.S. Pettit: *Introduction to the High Temperature Oxidation of Metals*, Cambridge University Press, Cambridge, 2006, pp. 207–14.
40. S. Kim, J. Chen, T. Cheng, A. Gindulyte, J. He, S. He, Q. Li, BA Shoemaker, PA Thiessen, B. Yu, L. Zaslavsky, J. Zhang, and EE Bolton: *Nucleic Acids Res.*, 2019, vol. 47 (1), pp. 1102–09.
41. G. Parashar, M. Bajpayee, and P.K. Kamani: *Surf. Coat. Int. Part B*, 2003, vol. 86, pp. 209–16.
42. D. Dimas, I. Giannopoulou, and D. Panias: *J. Mater. Sci.*, 2009, vol. 44, pp. 3719–30.
43. E. Sampson and S. Sridhar: *Metall. Mater. Trans. B*, 2013, vol. 44B, pp. 1124–36.
44. K. Matsumoto, M. Izawa, T. Nakanishi, and K. Tsubouchi: *Tribol. Trans.*, 2009, vol. 52, pp. 553–59.
45. R.Y. Chen and W.Y.D. Yeun: *Oxid. Met.*, 2003, vol. 59, pp. 433–68.
46. H.F. Marston, P.H. Bolt, G. Leprince, M. Röder, R. Klima, J. Niska, and M. Jarl: *Ironmak. Steelmak.*, 2004, vol. 31, pp. 57–65.
47. D. Caplan, G.I. Sproule, R.J. Hussey, and M.J. Graham: *Oxid. Met.*, 1968, vol. 12, pp. 67–82.
48. H.V. Makar and B.W. Dunning: *JOM*, 1969, vol. 21, pp. 19–22.
49. W. Yang: The structure and properties of mill scale in relation to easy removal, Doctoral Dissertation, University of Sheffield, 2001.
50. H. Tanei and Y. Kondo: Nippon Steel & Sumitomo Metal Technical Report No. 111, 2016.
51. E.B. Schneider: U.S. Patent No. 3,178,322, 1965.
52. S. Ye, L. Wei, Y. Xie, Y. Chen, J. Qiu, D. Zou, and Y. Zou: U.S. Patent No. 7,494,692, 2009.
53. M. Galopin and J.S. Daniel: *Electrodepos. Surf. Treat.*, 1975, vol. 3, pp. 1–31.
54. P.J.W.K. de Buzin, N.C. Heck, and A.C.F. Vilela: EAF dust *J. Mater. Res. Technol.*, 2017, vol. 6, pp. 194–202.
55. M. Östman, K. Lundkvist, and M. Larsson: *World Renewable Energy Congress-Sweden*, No. 57, pp. 1684–91.
56. G.F. Porzio, V. Colla, B. Fornai, M. Vannucci, M. Larsson, and H. Stripple: *Appl. Energy*, 2016, vol. 161, pp. 656–72.
57. Z. Yao, J. Li, and X. Zhao: *Chemosphere*, 2011, vol. 84, pp. 1167–74.

**Publisher's Note** Springer Nature remains neutral with regard to jurisdictional claims in published maps and institutional affiliations.